Published in final edited form as:
Biochemistry. 2011 July 26; 50(29): 6308–6311. doi:10.1021/bi200681q.

S_1-State Model of the O_2-Evolving Complex of Photosystem II

Sandra Luber[1,*], **Ivan Rivalta**[1], **Yasufumi Umena**[2], **Keisuke Kawakami**[3], **Jian-Ren Shen**[4], **Nobuo Kamiya**[3], **Gary W. Brudvig**[1], and **Victor S. Batista**[1,*]

[1]Department of Chemistry, Yale University, New Haven, Connecticut, 06520-8107, USA

Abstract

We introduce a Quantum Mechanics/Molecular Mechanics model of the oxygen-evolving complex (OEC) of photosystem II in the S_1 Mn_4(IV, III, IV, III) state, where Ca^{2+} is bridged to manganese centers by the carboxylate moieties of D170 and A344 based on the new X-ray diffraction (XRD) model recently reported at 1.9 Å resolution. The model is also consistent with high-resolution spectroscopic data, including polarized extended X-ray absorption fine structure data of oriented single crystals. Our results provide refined intermetallic distances within the Mn cluster and suggest that the XRD model most likely corresponds to a mixture of oxidation states, including more reduced species than observed in the catalytic cycle of water splitting.

Keywords

Photosystem II; Oxygen-Evolving Complex; EXAFS; DFT QM/MM

Photosystem II (PSII) is a transmembrane protein complex with about 20 protein subunits, several electron-transfer quinone factors, and a photo-antenna system of chlorophyll and carotenoid pigments. Of special interest is the oxygen-evolving complex (OEC), which contains a $CaMn_4$ cluster that catalyzes the oxidation of water to produce dioxygen (1-5). In contrast to (electro)-chemical water splitting, direct solar water oxidation by the OEC requires only moderate activation energies and features high turnover rates that are still unmatched by artificial water splitting systems. Elucidating its molecular structure is thus an important prerequisite for a detailed understanding of the catalytic cycle and the development of biomimetic catalysts.

A variety of spectroscopic methods have been applied to study the OEC including mass spectrometry (6, 7), Fourier transform (FT) infrared spectroscopy (8), electron paramagnetic resonance spectroscopy (9, 10), and X-ray diffraction (XRD) (11-16). Until recently, XRD data were available only at moderate resolution (11-15), leaving uncertainty on the exact position of the manganese atoms, water molecules, and coordination of the surrounding ligands. Nevertheless, tentative OEC models were proposed on the basis of the XRD density maps and high-resolution spectroscopic data. The recent breakthroughs in XRD provide for the first time data at 1.9 Å resolution (16, 17), suggesting a cuboidal structure similar to

*sandra.luber@yale.edu; victor.batista@yale.edu; phone: +1 (203)-432-6672; fax: +1 (203) 432-6144 .
[2]Current Address: Institute for Protein Research, Osaka University, 3-2 Yamadaoka, Suita-shi, Osaka 565-0871, Japan
[3]Current Address: Department of Chemistry, Graduate School of Science, and The OCU Advanced Research Institute for Natural Science and Technology (OCARINA), Osaka City University, Sumiyoshi, Osaka 558-8585, Japan
[4]Current Address: Division of Bioscience, Graduate School of Natural Science and Technology/Faculty of Science, Okayama University, 1-1, Naka 3-chome, Tsushima, Okayama 700-8530, Japan.

BRIEFS. Model of the resting state of the OEC of PSII.

SUPPORTING INFORMATION AVAILABLE Description of computational methods. This material is available free of charge via the Internet http://pubs.acs.org.

previous models, although with a ligation scheme in which Ca^{2+} is bridged to Mn centers by the carboxylate moieties of D170 and A344 centers (see Figure 1). These results offer a great opportunity to establish a structural model of the OEC in the resting or so-called storage-state (S-state) S_1. Such a model should be particularly valuable for understanding the catalytic mechanism of water splitting in PSII.

Previous studies have proposed high-resolution extended X-ray absorption fine structure (EXAFS) measurements to rule out structural models of the OEC that did not match the isotropic and crystal-orientation-dependent polarized data (18,19,22). In addition, several models of the OEC core, which are consistent with experimental EXAFS spectra, have been proposed (22). Moreover, complete models, including the coordination of surrounding ligands based on the 1S5L crystal structure (13) have also been shown to agree with EXAFS data. In fact, it has been possible to derive OEC models from Quantum Mechanics (QM)/ Molecular Mechanics (MM) calculations using density functional theory (DFT) (23-25) for the S-state intermediates along the catalytic cycle, S_0, S_1, S_2, S_3 and S_4. In addition, an S_1-state model matching polarized experimental EXAFS data has been obtained by refining the structure of the optimized QM/MM model (23). This has been achieved by minimizing a score function based on the root mean square deviations of the experimental and calculated polarized EXAFS spectra. The resulting refinement could also be achieved by QM optimization biased by deviations between simulated and experimental EXAFS spectra (26). Here, we report for the first time the analogous DFT-QM/MM model based on the ligation scheme determined by the new X-ray model as well as its EXAFS-refined structure. The DFT-QM/MM model is built by using the two-layer ONIOM link-hydrogen atom approach, implemented in *Gaussian 09* (27), as in our previous studies (23-25). The preparation of the initial electronic state is based on high-quality spin-electronic states for the ligated cluster of Mn ions using *Jaguar v.7.7* (28). Geometry optimized structures were obtained under the constraint of fixed alpha carbon atoms (for details, see Supplementary Material) as determined by the coordinates in the new XRD model. EXAFS spectra were calculated using the ab initio real space Green function approach in the program FEFF (version 8.30), employing the coordinates of the Mn_4Ca cluster and surrounding ligands provided by the model system of interest.

Figure 2 shows that the isotropic EXAFS spectrum calculated for the new XRD model is significantly different from the experimental spectrum (19, 20) of the S_1 state. This is likely due to the fact that the XRD model does not have any Mn-Mn distance shorter than 2.8 Å in chain A. While the comparison to the S_0 state is more favorable, there is no quantitative agreement with any S-state intermediate. This could be due to reductive damage caused by the high doses of X-ray radiation (21), leading to a mixture of reduced S-states, or simply structural disorder (in the absence of radiation damage for PSII crystallized as a mixture of S-state intermediates along the catalytic cycle). While the former possibility is likely to be the case, the latter is ruled out by comparing the calculated spectrum of the XRD model to weighted averages of experimental S_0, S_1, S_2, and S_3 spectra (see Supporting Information). Even mixtures with the best possible fit (e.g., including ~60% of the S_0 intermediate) do not generate average spectra in quantitative agreement with the spectrum of the XRD model. These results suggest that the coordinates of the new X-ray model do not correspond to any S_0-S_3 intermediate, or mixture of solely those intermediate states, but may contain also pre-S_0 state intermediates such as S_{-1} and S_{-2}. Other causes may be experimental errors (0.16 Å) in the XRD model as well as a different combination of spin states of the metal ions and protonation states of the ligands.

Figure 3 shows the experimental isotropic (19, 20) and polarized (22) EXAFS spectra for the S_1 state, as compared to the corresponding spectra calculated for the DFT-QM/MM model of the OEC. This model is based on the new XRD model, where the dangling Mn(4) is

bridged to Ca by the carboxylate moiety of D170. The oxidation state Mn_4(IV, III, IV, III) is predicted with the BP86 (29, 30) and B3LYP (31, 32) density functionals. Intermetallic distances, given in Table 1, and Mulliken atomic spin densities for Mn(1)=−2.9(−2.7), Mn(2)=3.9(3.8), Mn(3)=2.9(2.6), and Mn(4)=−3.9(−3.6) (for numbering of atoms, see Figure 1) are consistent with high-resolution spectroscopy. The resulting model gives isotropic and polarized EXAFS spectra in good agreement with experimental data. The directly bound ligands (D170, A344, E189, E354, E333, D342) and μ-oxo-bridges are unprotonated, while all water ligands are H_2O (compare left-hand side of Figure 4 for a picture of the DFT-QM/MM model obtained with the B3LYP density functional).

To obtain a model of the OEC in quantitative agreement with high-resolution spectroscopic data, we implemented an EXAFS structural refinement scheme as reported in earlier work (23). We refined the DFT-QM/MM model by iteratively adjusting the nuclear coordinates to minimize a scoring function defined as the sum of the squared deviations between calculated and experimental EXAFS spectra, plus a quadratic penalty factor that ensures minimum displacements of the nuclear positions relative to the reference configuration. As shown in Figure 3, the resulting configuration of the R-QM/MM model yields isotropic and polarized EXAFS data in quantitative agreement with experiments. As mentioned in previous work (23), however, the agreement with high-resolution spectroscopic data does not rule out other possible structures since the model is a *local* solution relative to the reference DFT-QM/MM structure. The comparison of the cuboidal structure of the OEC in the new DFT-QM/MM model (obtained from the B3LYP density functional), and the 2006 DFT-QM/MM model (25) based on the XRD model at 3.5 Å resolution is shown in Figure 4 and the complete comparison of intermetallic distances in the models of the OEC of PSII is reported in Table 1, including the new XRD structure at 1.9 Å resolution, the new DFT-QM/MM model of the OEC in the S_1 state, the new R-QM/MM, and the 2006 DFT-QM/MM structure. While there are similarities between the various models, there are also significant differences, including the new D170 bridge between Ca and Mn(4), shortening the Mn(3)-Mn(4) and elongating the Mn(2)-Mn(3) distances when compared to the 2006 DFT-QM/MM structure.

In summary, we have introduced a DFT-QM/MM model of the OEC of PSII in the S_1 Mn_4(IV, III, IV, III) state, with a ligation scheme consistent with the new XRD model, where Ca^{2+} is bridged to Mn centers by the carboxylates of D170 and A344. In contrast to the XRD model, the DFT-QM/MM structure is fully consistent with high-resolution spectroscopic data, including polarized-EXAFS spectra of oriented single crystals, suggesting that the XRD model corresponds to a mixture of states, most likely including S_0 and pre-S_0 intermediates S_{-1}, S_{-2}. The revised DFT-QM/MM structure should be particularly relevant to the analysis of S-state intermediates consistent with the ligation scheme proposed by the new XRD model.

Supplementary Material

Refer to Web version on PubMed Central for supplementary material.

Acknowledgments

V.S.B acknowledges financial support from the Division of Chemical Sciences, Geosciences, and Biosciences, Office of Basic Energy Sciences of the U.S. Department of Energy (DE-SC 000-1423), supercomputer time from NERSC and support from the NIH Grant GM84267 for the development of methods implemented in this study. G.W.B acknowledges support from the NIH grant GM32715.

REFERENCES

(1). McEvoy JP, Brudvig GW. Chem. Rev. 2006; 106:4455–4483. [PubMed: 17091926]

(2). Diner, BA.; Babcock, GT. Oxygenic photosynthesis: the light reactions. Kluwer Academic Publishers; Dordrecht, The Netherlands: 1996. p. 213-247.

(3). Britt, RD. Oxygenic photosynthesis: the light reactions. Kluwer Academic Publishers; Dordrecht, The Netherlands: 1996. p. 137-164.

(4). Witt H. Ber. Bunsen-Ges. Phys. Chem. 1996; 100:1923–1942.

(5). Debus RJ. Biochim. Biophys. Acta. 1992; 1102:269–352. [PubMed: 1390827]

(6). Hillier W, Wydrzynski T. Phys. Chem. Chem. Phys. 2004; 6:4882–4889.

(7). Messinger J, Badger M, Wydrzynski T. Proc. Natl. Acad. Sci. U. S. A. 1995; 92:3209–3213. [PubMed: 11607525]

(8). Chu H, Hillier W, Debus R. Biochemistry. 2004; 43:3152–3166. [PubMed: 15023066]

(9). Peloquin J, Campbell K, Randall D, Evanchik M, Pecoraro V, et al. J. Am. Chem. Soc. 2000; 122:10926–10942.

(10). Kulik L, Epel B, Lubitz W, Messinger J. J. Am. Chem. Soc. 2005; 127:2392–2393. [PubMed: 15724984]

(11). Biesiadka J, Loll B, Kern J, Irrgang K, Zouni A. Phys. Chem. Chem. Phys. 2004; 6:4733–4736.

(12). Kamiya N, Shen J. Proc. Natl. Acad. Sci. U. S. A. 2003; 100:98–103. [PubMed: 12518057]

(13). Ferreira KN, Iverson TM, Maghlaoui K, Barber J, Iwata S. Science. 2004; 303:1831–1838. [PubMed: 14764885]

(14). Loll B, Kern J, Saenger W, Zouni A, Biesiadka J. Nature. 2005; 438:1040–1044. [PubMed: 16355230]

(15). Guskov A, Kern J, Gabdulkhakov A, Broser M, Zouni A, et al. Nat. Struct. Mol. Biol. 2009; 16:334–342. [PubMed: 19219048]

(16). Umena Y, Kawakami K, Shen J-R, Kamiya N. Nature. 2011; 473:55–60. [PubMed: 21499260]

(17). Kawakami K, Kamiya N, Shen J-R. J. Photochem. Photobiol. B. 2011; 104:9–18. [PubMed: 21543235]

(18). Grabolle M, Haumann M, Muller C, Liebisch P, Dau H. J. Biol. Chem. 2006; 281:4580–4588. [PubMed: 16352605]

(19). Haumann M, Muller C, Liebisch P, Iuzzolino L, Dittmer J, et al. Biochemistry. 2005; 44:1894–1908. [PubMed: 15697215]

(20). Dau H, Liebisch P, Haumann M. Phys. Chem. Chem. Phys. 2004; 6:4781–4792.

(21). Yano J, Kern J, Irrgang K, Latimer M, Bergmann U, et al. Proc. Natl. Acad. Sci. U. S. A. 2005; 102:12047–12052. [PubMed: 16103362]

(22). Yano J, Kern J, Sauer K, Latimer MJ, Pushkar Y, et al. Science. 2006; 314:821–825. [PubMed: 17082458]

(23). Sproviero EM, Gascon JA, McEvoy JP, Brudvig GW, Batista VS. J. Am. Chem. Soc. 2008; 130:6728–6730. [PubMed: 18457397]

(24). Sproviero EM, Gascon JA, McEvoy JP, Brudvig GW, Batista VS. J. Am. Chem. Soc. 2008; 2:3428–3442. [PubMed: 18290643]

(25). Sproviero EM, Gascon JA, McEvoy JP, Brudvig GW, Batista VS. J. Chem. Theory Comput. 2006; 2:1119–1134.

(26). Hsiao Y-W, Tao Y, Shokes JE, Scott RA, Ryde U. Phys. Rev. B. 2006; 74:214101.

(27). Frisch MJ, Trucks GW, Schlegel HB, Scuseria GE, Robb MA, et al. Gaussian 09. 2009

(28). Jaguar 7.7. Schroedinger, LLC; New York, NY: 2010.

(29). Becke AD. Phys. Rev. A. 1988; 38:3098–3100. [PubMed: 9900728]

(30). Perdew JP. Phys. Rev. B. 1986; 33:8822–8824.

(31). Becke AD. J. Chem. Phys. 1993; 98:5648–5652.

(32). Lee C, Yang W, Parr RG. Phys. Rev. B. 1988; 37:785–789.

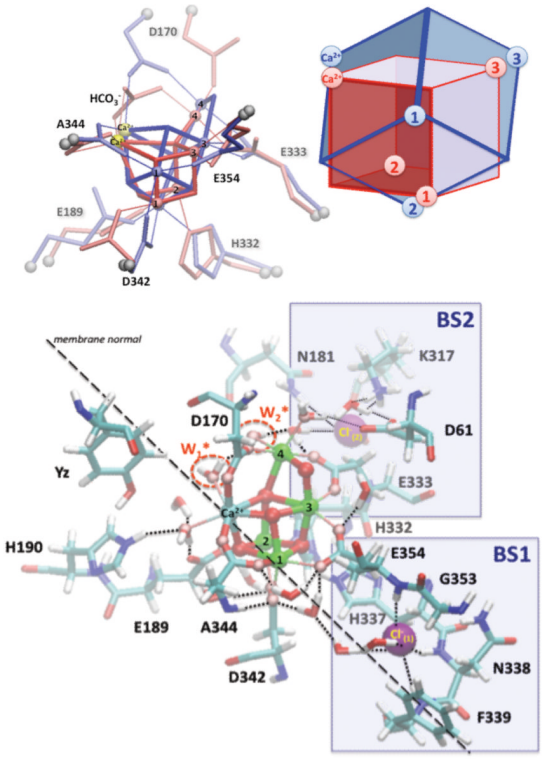

FIGURE 1.

(Top) Superposition of the OEC in the X-ray models of PSII at 1.9 Å (blue) (16, 17) and 3.5 Å (red) (13) resolution. (Bottom) Ligation scheme with D170 bridging between Mn(4) and Ca, and chloride binding sites (BS1 and BS2) as proposed by the X-ray model at 1.9 Å resolution.

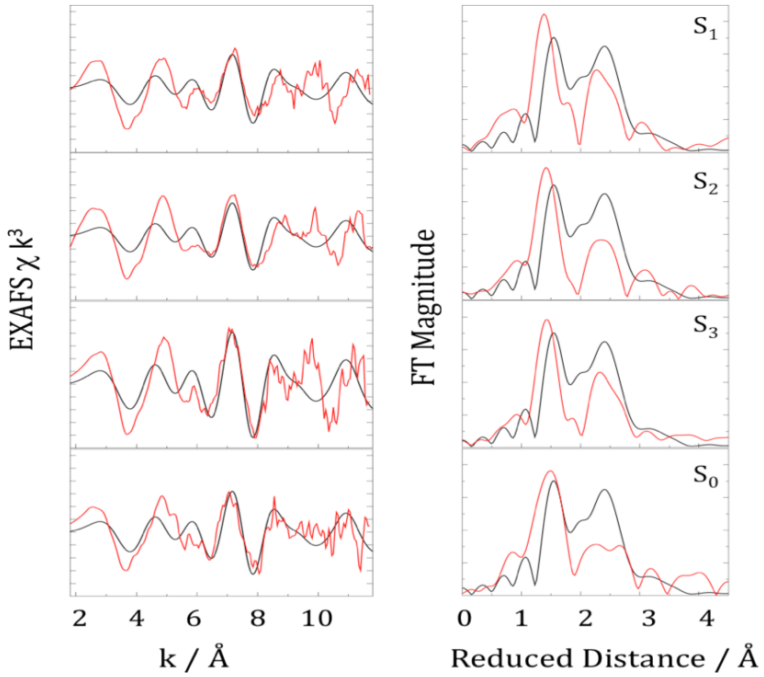

FIGURE 2.

Comparison between experimental (red) (19, 20) k^3-weighted EXAFS spectra (left) and Fourier transform (FT) magnitudes (right) for the OEC of PSII in the S_0-S_3 states and the simulated (black) spectrum for the new X-ray model (chain A) at 1.9 Å resolution. Reduced space spectra show prominent peaks corresponding to scattering centers in the first (O, N), second (Mn in the core), and third (dangling Mn, Ca) coordination shells of Mn.

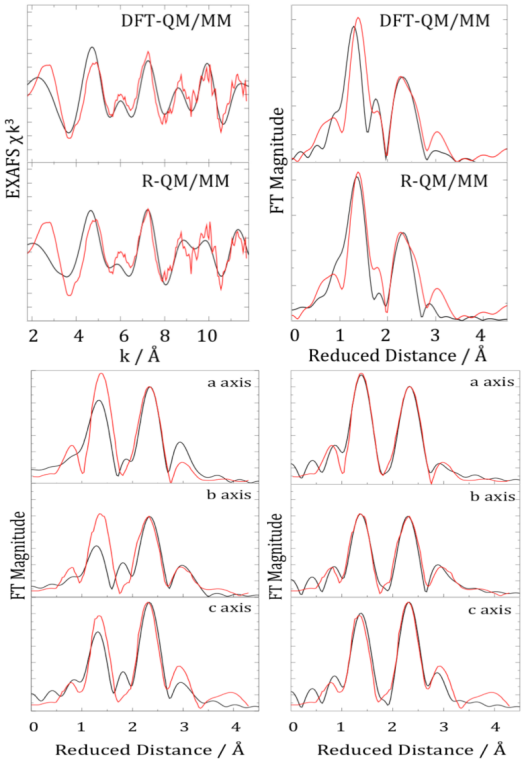

FIGURE 3.

Comparison between experimental (red) (19, 20,22) and calculated (black) isotropic (upper two rows) and polarized (lower part) EXAFS spectra for the OEC of PSII in the S_1 state calculated from the new DFT-QM/MM and refined R-QM/MM model.

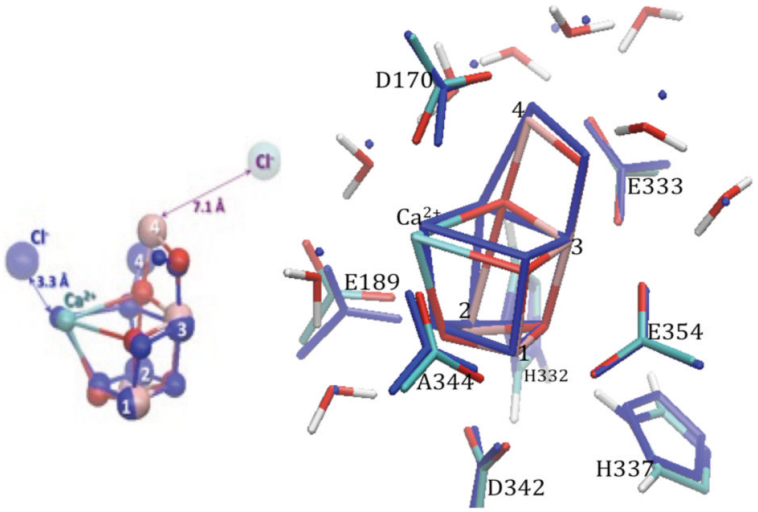

Figure 4.

Left: Comparison of the new DFT QM/MM model of the OEC of PSII in the S_1 state (colors) and the 2006 DFT QM/MM model (blue). Right: the X-ray model at 1.9 Å resolution (blue) and the new DFT-QM/MM model (colors).

Table 1

Intermetallic distances (Å) in the X-ray model (chain A/a) (16), compared to the new DFT-QM/MM model obtained with the density functional B3LYP (BP86), the refined R-QM/MM model and the 2006 DFT-QM/MM model (25).

	X-ray A/a	QM/MM B3LYP(BP86)	R-QM/MM	2006-QM/MM
Mn(1)-Mn(2)	2.84/2.76	2.80 (2.81)	2.76	2.76
Mn(1)-Mn(3)	2.89/2.91	2.80 (2.80)	2.71	2.76
Mn(2)-Mn(3)	3.29/3.30	3.38 (3.38)	3.25	2.82
Mn(3)-Mn(4)	2.97/2.91	2.75 (2.74)	2.76	3.72
Mn(2)-Mn(4)	5.00/4.95	4.89 (4.88)	4.68	3.34
Ca-Mn(2)	3.51/3.46	3.56 (3.52)	3.52	3.31
Ca-Mn(3)	3.41/3.44	3.62 (3.59)	3.49	3.95
Ca-Mn(1)	3.36/3.29	3.35(3.36)	3.38	3.59
Ca-Mn(4)	3.79/3.80	3.81(3.77)	3.67	3.84